frontiers | Frontiers in Physics

TYPE Brief Research Report
PUBLISHED 01 December 2022
DOI 10.3389/fphy.2022.1084594

OPEN ACCESS

EDITED BY
Zhi-Han Zhu,
Harbin University of Science and Technology, China

REVIEWED BY
Song Yang,
Technical University of Denmark, Denmark
Fei Wang,
Changchun University of Science and Technology, China

*CORRESPONDENCE
Zhenao Bai,
baizhenao@hotmail.com
Weiguo Wang,
wangwei5878@sina.com

SPECIALTY SECTION
This article was submitted to Optics and Photonics, a section of the journal Frontiers in Physics

RECEIVED 30 October 2022
ACCEPTED 22 November 2022
PUBLISHED 01 December 2022

CITATION
Zhang Z, Bai Z, Song X, Zhang Y, Liang B, Liu T and Wang W (2022), 178-W picosecond green laser with active beam-pointing stabilization. *Front. Phys.* 10:1084594. doi: 10.3389/fphy.2022.1084594

178-W picosecond green laser with active beam-pointing stabilization

Zhendong Zhang[1], Zhenao Bai[2]*, Xiaoquan Song[3], Yakai Zhang[4], Bo Liang[5], Tingxia Liu[1] and Weiguo Wang[1]*

[1]Changchun Institute of Optics, Fine Mechanics and Physics, Chinese Academy of Sciences, Changchun, China, [2]Aerospace Information Research Institute, Chinese Academy of Sciences, Beijing, China, [3]China Aerospace Academy of Systems Science and Engineering, Beijing, China, [4]Center for Advanced Laser Technology, Hebei University of Technology, Tianjin, China, [5]The Military Representative Office in Changchun of Military Representative Bureau of Space System Equipment Department, Changchun, China

Picosecond lasers with high average power and high beam quality have been widely used for precision processing and space exploration. In this study, we report a high-power picosecond green laser using a multistage Yb-doped rod-shaped photonic crystal fiber as an amplifier combined with a beam combination. The single amplification module achieves a 1,030 nm laser output of 146.8 W, and the maximum second harmonic generation (SHG) power is 92 W with a frequency conversion efficiency of 63.5%. The combined beam of the two SHGs resulted in a final output of 178 W with a repetition frequency of 24.07 MHz, pulse width of 50.1 ps, and beam quality factor of M^2 = 1.16. Furthermore, an adaptive filter control method of a two-axis fast-steering mirror was applied to suppress the beam jitter to up to 45 Hz.

KEYWORDS

photonic crystal fiber, picosecond amplifiers, second harmonic generation, beam jitter suppression, beam-pointing stabilization

Introduction

High-power laser sources with high beam quality and spectral diversity are of broad interest for various applications [1–5]. Among them, ultrashort pulse (picosecond and femtosecond) lasers are widely used in industrial processing, precision manufacturing, and waveguide etching because of their negligible heat-affected zones [6–10]. Compared to nanosecond pulses, picosecond lasers have a higher peak power that can control the processing depth and precision more effectively and greatly improve the processing quality [11–13]. Meanwhile, compared to femtosecond pulses, picosecond lasers achieve high-power output with higher stability easier [14–17]. In addition to achieving a high-power output, short-pulse lasers at specific wavelengths are also necessary for various applications. For example, the need for green picosecond pulsed lasers is also more widespread, as many materials in industrial processes absorb visible light more significantly than infrared light and in marine and space exploration, where the transmission medium absorbs less of the green wavelength [18–21]. Currently,

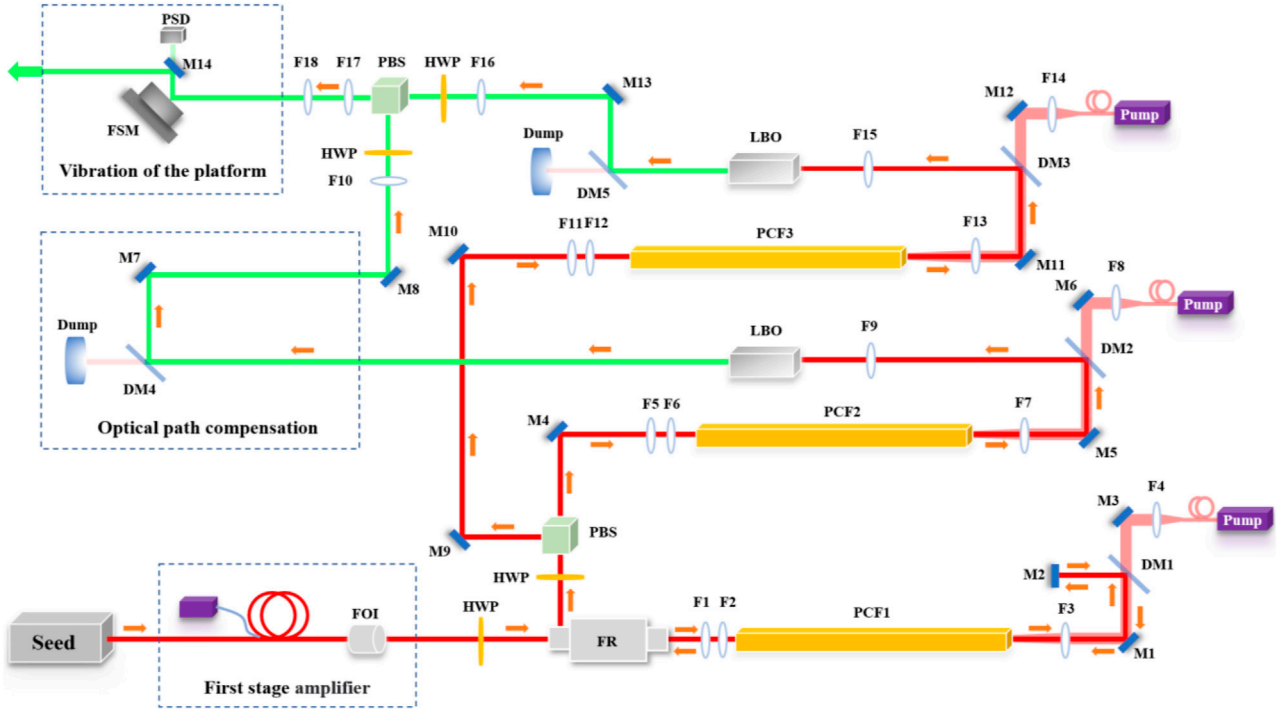

FIGURE 1
Schematic showing the layout of the laser system. FOI, fiber optic isolator; HWP, half-wave plate; FR, Faraday rotator; M, mirrors; F, focus lens; PBS, polarizing beam splitter. FSM, fast steering mirror; PSD, position sensitive detector.

picosecond pulses can be amplified by rod-tape photonic crystal fibers (PCF), which can achieve extremely high amplification efficiency, polarization preservation, and excellent beam quality output [22–24]. Its difference from traditional optical fiber, with its characteristics of cut-off-free single-mode transmission, adjustable dispersion, high birefringence, large mode area, and high nonlinearity coefficient, realizes single-mode transmission in the large mode field of optical fiber, which makes a breakthrough in high peak power transmission and amplification of optical fiber [24–26]. In addition, beam jitter is an issue that must be addressed to extend the application of lasers to moving platforms such as aircraft, ships, vehicles, and satellites [27, 28]. Beam jitter caused by engine vibration, atmospheric turbulence, and attitude changes severely limits the pointing performance of laser beams on moving platforms [29].

In this study, we report a picosecond amplification structure using a multi-stage Yb-doped rod-shaped PCF, divided into a two-stage pre-amplification and a one-stage main amplification structure. The single main amplification module finally achieves a 1,030 nm laser output of 146.8 W. The frequency doubling crystal is an LiB_3O_5(LBO) crystal, and the output second harmonic generation (SHG) wavelength was 514.2 nm with a maximum output power of 92 W. The conversion efficiency from 1,030 nm to 514.2 nm was 63.5%. The two SHGs were combined to obtain a final output of 178 W at 514.2 nm. The repetition frequency of the laser is 24.07 MHz, pulse duration is 50.1 ps, and beam quality factor M^2 is measured to be 1.16. An adaptive filtering control method is applied to suppress the beam jitter of a two-axis fast-steering mirror (FSM) to increase the output stability. The FSM, driven by a voice coil driver, is placed in the optical path in front of the laser exit to isolate the laser beam from the disturbance. Using a position-sensitive detector (PSD) as a beam deviation sensor, the system effectively suppresses laser beam jitter up to 45 Hz, resulting in a high pointing stability of 178 W green light output.

Experiment and results

The laser amplification and frequency doubling experimental setup are shown in Figure 1, which consists of a pre-amplification module, main amplification module, frequency doubling module, and optical range compensation module. The mode-locked fiber laser (EOAS-MLFL-P-50-22-1,030-50) outputs seeds with a repetition frequency of 22 ± 2 MHz, pulse duration of 50 ± 2.5 ps, and central wavelength of 1,030 ± 1 nm. The output seed light is amplified by a primary fiber prevention module, which aims to increase the efficiency of the photonic crystal fiber amplifier (PCFA) afterward. The amplified seed light then

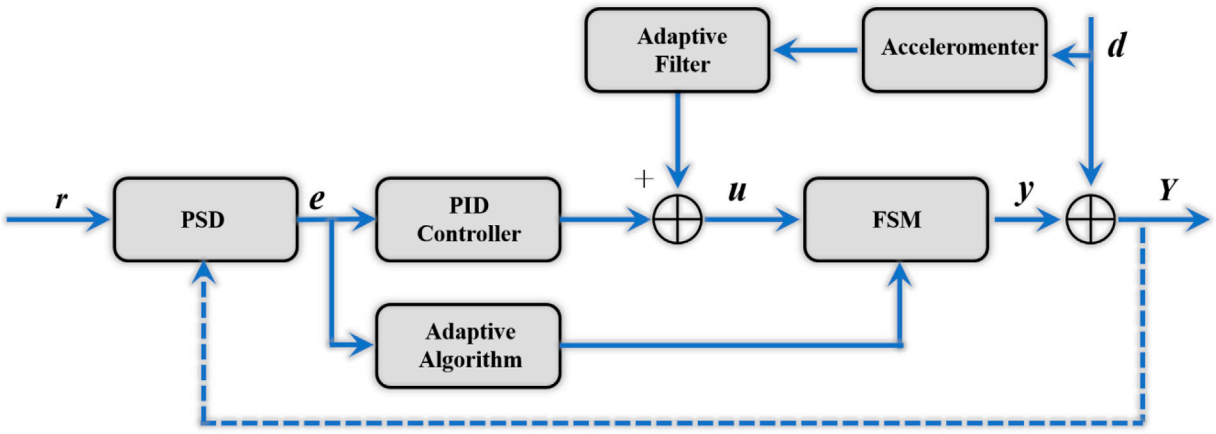

FIGURE 2
Controller schematic of adaptive in parallel with PID.

passes through the optical isolator as signal light into the secondary PCF preamplifier. In secondary pre-amplification, the signal light is collimated and focused by a coupling lens set and then injected into a rod-taped PCF, where the PCF is pumped by a fiber-coupled diode with a central wavelength of 976 nm, and the pumped light is collimated and focused into the PCF.

In the PCF (aeroGAIN-ROD-2.1, mode field diameter 65 ± 5 μm), the signal light receiving core diameter is approximately 85 μm, and after passing through the coupling lens set, the signal light matches the receiving core diameter by more than 90%. The pump light receiving diameter is 260 μm, and after passing through the coupling lens set, the pump light spot with a diameter of 200 μm and NA = 0.22 was injected into the PCF with a 1:1 coupling ratio to achieve 95% energy within 250 μm. After secondary pre-amplification, the 1,030 nm laser was split into two beams using a half-wave plate and a polarization splitting prism for respective amplification and frequency doubling. The split beam was first coupled through a coupling lens set to the PCF for single-pass amplification. The signal light and pump light coupling system of the rod-tape PCF was identical to that of the secondary preamplification module.

The signal light is amplified again and then passed through the focusing lens as the fundamental frequency light for frequency doubling. The frequency-doubling crystal was an LBO crystal (type I, 3 mm × 3 mm × 15 mm) with a combination of angle and temperature matching, a cut angle of $\theta = 90^{\circ}$, $\varphi = 12.6^{\circ}$, and a corresponding temperature of 55°C. The advantage of this is that the best matching efficiency can be obtained while avoiding strong convection owing to large temperature gradients, which can affect the output light stability. A dichroic mirror was then used to separate 1,030 nm from the SHG, which was collected by a collector, and the SHG was then combined. Before the beam combining process, one of the beams needs to be compensated for the optical range to match the temporal overlap of the two beams. After passing through a collimating lens and half-wave, the two SHGs are combined in a polarizing beam-splitting prism and then collimated and expanded into the beam jitter suppression module.

Beam jitter suppression experiments were performed after the green laser was output. The experimental optical path is shown in Figure 1, where a two-axis FSM driven by a voice coil driver is placed in the optical path behind the laser exit, with the laser placed on a jitter platform. A small portion of the laser beam was split into the PSD by adding a semi-transparent and semi-reflective mirror to the beam path. By using the PSD as a beam deviation sensor, the FSM effectively suppresses laser beam dithering. The controller program design is shown in Figure 2. The principle is that when the system is switched on, the reference signal contains a large direct-current component, which can destabilize the adaptive filter. Therefore, a proportional-integral-derivative (PID) controller was adopted in parallel with the adaptive filter to stabilize the entire controller. As shown in Figure 2, once the PID controller is connected in parallel with the adaptive filter, the initial bias error is eliminated, and the adaptive filter works properly. In the experiment, the vibration platform generated a broadband disturbance signal with a frequency of 0–50 Hz to test the stabilization effect of the controller.

In our experiment, the signal power after the second-stage pre-amplification was 80 W, and the pump power was 162 W. In one of the main amplification stages, the output power increased linearly as the pump power increased, and the conversion efficiency first increased and then plateaued, as shown in Figure 3A. At the maximum pump power of 360 W,

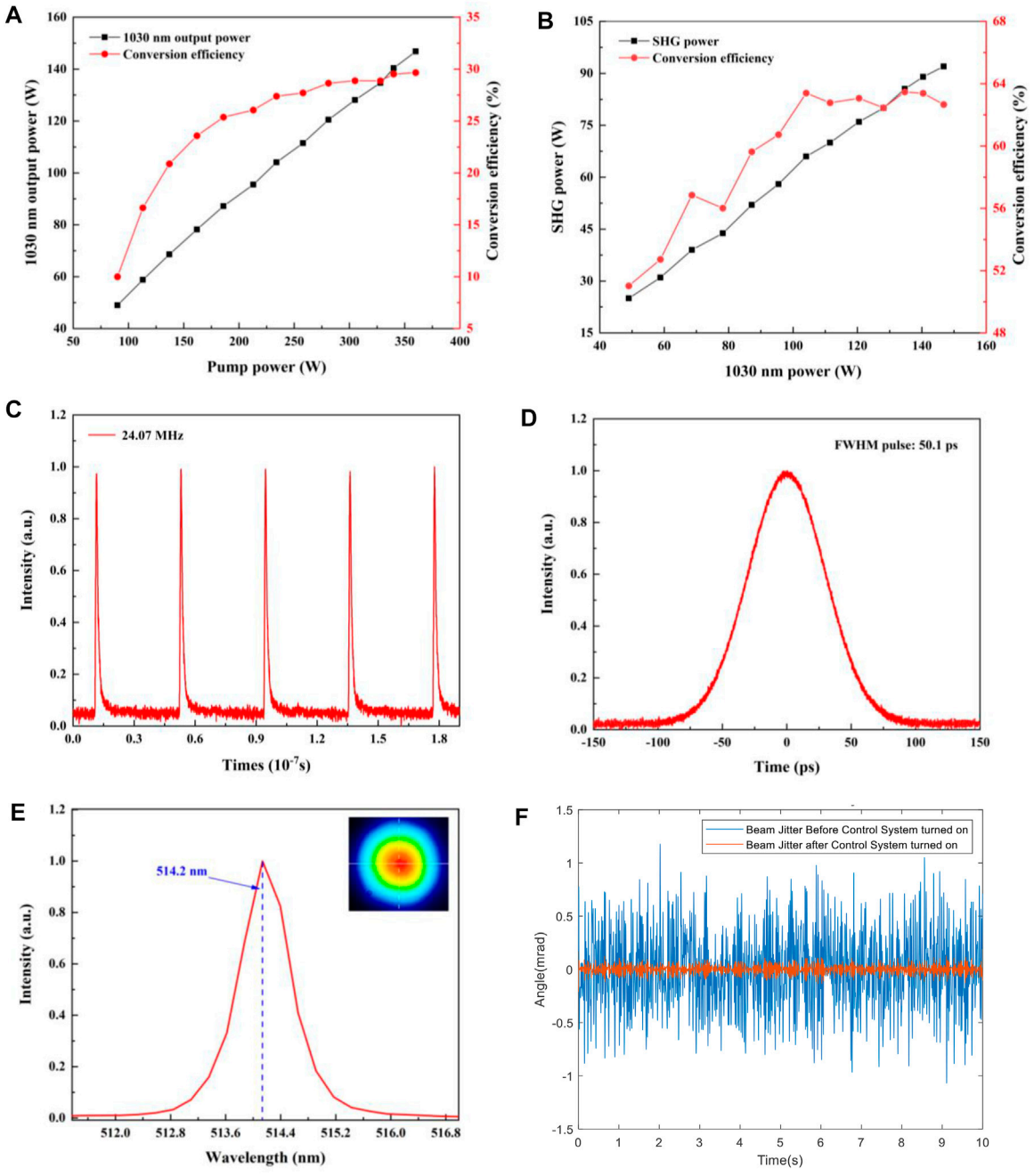

FIGURE 3
Compilation of output characteristics of the green laser. **(A)** 1,030 nm output power plotted against the pump power; **(B)** output SHG power at 512 nm plotted against the 1,030 nm input power; **(C)** Normalized pulse characteristics of the output with a close-up shown inset; **(D)** temporal characteristic of a single output pulse with an autocorrelation trace; **(E)** normalized wavelength spectrum of the amplified laser output; **(F)** Beam jitter before and after control system turned on.

maximum power of 146.8 W was obtained for the 1,030 nm output with an optical-to-optical conversion efficiency of 29.7%. By designing the coupling lens set for the signal and pump lights, more signal light can enter the fiber bar core, which can effectively suppress amplified spontaneous emission (ASE) and enable the fiber bar to obtain a higher gain, while a good coupling spot can also effectively improve the quality of the amplified beam. The output power of the amplification device has not yet reached saturation, and there is room for further improvement owing to the pumping power of the diode. Figure 3B shows the

output power curve of the SHG with the pump power. From the figure, it can be observed that the output power of the second harmonic increases as the pump power increases, and the maximum power of 92 W is obtained at the 1,030 nm power of 146.8 W for SHG output. The frequency conversion efficiency increases first, saturating at a 1,030 nm power of 104.1 W. The highest conversion efficiency occurs at the pumping power of 134.7 W, with a conversion efficiency of 63.5%. Subsequently, as the power increased, the efficiency decreased slightly, although the output power increased. This is partly due to the broadening of the 1,030 nm spectrum caused by the increase in laser power, partly due to the change in the divergence angle of the amplified beam, and partly due to the increased thermal effect of the doubled crystal caused by the increase in power. However, the results of the experiments were approximately the same as those mentioned above. At the maximum pump power of 360 W, 131 W of 1,030 nm laser output was output, and after the frequency-doubling crystal, 86 W of SHG was output, with a frequency doubling efficiency of 65.6%. The two frequency-doubled beams were combined to obtain a laser output of 178 W at 514 nm. The final output frequency of the SHG was 24.07 MHz with a pulse width of 50.1 ps, as shown in Figures 3C,D. The spectra measured using the spectrometer are shown in Figure 3E. The central wavelength was 514.2 nm. In the case of amplification, the fundamental mode signal light in the core is fully amplified owing to the cut-off-free single-mode characteristics of the fiber rod, whereas the light escaping into the cladding is not amplified. A larger core-cladding power ratio results in a higher beam quality of the output light, $M^2 = 1.16$. The vibration platform generated a broadband disturbance signal with frequencies ranging from 0 Hz to 50 Hz. With the use of the jitter suppression system, the jitter was effectively suppressed by approximately 18.4 dB, as shown in Figure 3F.

Conclusion

In this study, the seed light was amplified using a multi-stage rod-tape photonic crystal fiber, and a two-way amplification structure was incorporated to reduce the effect of thermal effects on the output light. The coupling system in the amplification module was designed independently to achieve mode-matching. The single amplification module achieves a 1,030 nm laser output of 146.8 W, and the maximum second harmonic generation (SHG) power is 92 W with a frequency conversion efficiency of 63.5%. After combining the beams, a green laser of 514.2 nm with a repetition frequency of 24.07 MHz, pulse width of 50.1 ps, and power of 178 W was output, with $M^2 = 1.16$. An adaptive filter control method for beam jitter suppression with a two-axis FSM was also applied to suppress laser beam jitter up to 45 Hz. The results can be used as a reference for the future realization of highly stable and miniaturized green picosecond pulsed lasers in the 100 W or even kW class for stable operation on mobile platforms.

Data availability statement

The raw data supporting the conclusion of this article will be made available by the authors, without undue reservation.

Author contributions

ZZ, Investigation, data analysis, and Writing-original draft preparation. ZB, Conceptualization, data analysis, Writing-review and editing, and funding acquisition. XS, Writing-review and editing. YZ, data analysis, Writing-original draft preparation, and Writing-review and editing. BL, Writing-review and editing. TL, Writing-review and editing. WW, Conceptualization and Supervision. All authors have read and agreed to the published version of the manuscript.

Funding

This work was supported by the Guangdong Key Research and Development Program (2018B090904003).

Conflict of interest

The authors declare that the research was conducted in the absence of any commercial or financial relationships that could be construed as a potential conflict of interest.

Publisher's note

All claims expressed in this article are solely those of the authors and do not necessarily represent those of their affiliated organizations, or those of the publisher, the editors and the reviewers. Any product that may be evaluated in this article, or claim that may be made by its manufacturer, is not guaranteed or endorsed by the publisher.

References

1. Jackson SD. Towards high-power mid-infrared emission from a fibre laser. *Nat Photon* (2012) 6(7):423–31. doi:10.1038/nphoton.2012.149

2. Fan ZW, Qiu JS, Kang ZJ, Chen YZ, Ge WQ, Tang XX. High beam quality 5 J, 200 Hz Nd: YAG laser system. *Light Sci Appl* (2017) 6(3):e17004. doi:10.1038/lsa.2017.4

3. Chen H, Bai Z, Yang X, Ding J, Qi Y, Yan B, et al. Enhanced stimulated Brillouin scattering utilizing Raman conversion in diamond. *Appl Phys Lett* (2022) 120(18):181103. doi:10.1063/5.0087092

4. Bai Z, Zhao Z, Tian M, Jin D, Pang Y, Li S, et al. A comprehensive review on the development and applications of narrow-linewidth lasers. *Microw Opt Technol Lett* (2022) 64(12):2244–55. doi:10.1002/mop.33046

5. Jin D, Bai Z, Lu Z, Fan R, Zhao Z, Yang X, et al. 22.5-W narrow-linewidth diamond Brillouin laser at 1064 nm. *Opt Lett* (2022) 47(20):5360–3. doi:10.1364/ol.471447

6. Wang X, Li C, Hong W, Ma C, Xing Y, Feng J. Fabrication of ordered hierarchical structures on stainless steel by picosecond laser for modified wettability applications. *Opt Express* (2018) 26(15):18998–9008. doi:10.1364/oe.26.018998

7. Esmail I, Yazdan Sarvestani H, Gholipour J, Ashrafi B. Engineered net shaping of alumina ceramics using picosecond laser. *Opt Laser Tech* (2021) 135:106669. doi:10.1016/j.optlastec.2020.106669

8. Qin Z, Ai J, Du Q, Liu J, Zeng X. Superhydrophobic polytetrafluoroethylene surfaces with accurately and continuously tunable water adhesion fabricated by picosecond laser direct ablation. *Mater Des* (2019) 173:107782. doi:10.1016/j.matdes.2019.107782

9. Guo B, Sun J, Lu Y, Jiang L. Ultrafast dynamics observation during femtosecond laser-material interaction. *Int J Extrem Manuf* (2019) 1(3):032004. doi:10.1088/2631-7990/ab3a24

10. Bai Z, Chen H, Gao X, Li S, Qi Y. Highly compact nanosecond laser for space debris tracking. *Opt Mater* (2019) 98:109470. doi:10.1016/j.optmat.2019.109470

11. Chichkov BN, Momma C, Nolte S, Alvensleben F, Tunnermann A. Femtosecond, picosecond, and nanosecond laser ablation of solids. *Appl Phys A Mater Sci Process* (1996) 63(2):109–15. doi:10.1007/bf01567637

12. Bai Z, Bai Z, Kang Z, Lian F, Lin W, Fan Z. Non-pulse-leakage 100-kHz level, high beam quality industrial grade Nd: YVO_4 picosecond amplifier. *Appl Sci* (2017) 7(6):615. doi:10.3390/app7060615

13. Qi Y, Yang S, Wang J, Li L, Bai Z, Wang Y, et al. Recent advance of emerging low-dimensional materials for vector soliton generation in fiber lasers. *Mater Today Phys* (2022) 23:100622. doi:10.1016/j.mtphys.2022.100622

14. Zhang Q, Zhao Y, Wei Z. Sub-10 fs laser pulses with repetition rate of 1.1 GHz by a Ti: Sapphire oscillator. *Chin Sci Bull* (2009) 54(20):3649–52. doi:10.1007/s11434-009-0191-6

15. Eckerle M, Dietrich T, Schaal F, Pruss C, Osten W, Ahmed MA, et al. Novel thin-disk oscillator concept for the generation of radially polarized femtosecond laser pulses. *Opt Lett* (2016) 41(7):1680–3. doi:10.1364/ol.41.001680

16. Li K, Wang Y, Yu Y, Yue J, Song C, Cao C, et al. Amplification of high repetition-rate, picosecond laser pulses using a zig-zag slab configuration. *Opt Laser Tech* (2023) 157:108717. doi:10.1016/j.optlastec.2022.108717

17. Hubka Z, Antipenkov R, Boge R, Erdman E, Greco M, Green JT, et al. 120 mJ, 1 kHz, picosecond laser at 515 nm. *Opt Lett* (2021) 46(22):5655–8. doi:10.1364/ol.440448

18. Peng R, Guo L, Zhang X, Li F, Cui Q, Bo Y, et al. 43W picosecond laser and second-harmonic generation experiment. *Opt Commun* (2009) 282(4):611–3. doi:10.1016/j.optcom.2008.10.049

19. Wang W, Liu J, Chen F, Li L, Wang Y. 532-nm picosecond pulse generated in a passively mode-locked Nd:YVO_4 laser. *Chin Opt Lett* (2009) 7(8):706–8. doi:10.3788/col20090708.0706

20. Cai Y, Gao F, Chen H, Yang X, Bai Z, Qi Y, et al. Continuous-wave diamond laser with a tunable wavelength in orange-red wavelength band. *Opt Commun* (2023) 528:128985. doi:10.1016/j.optcom.2022.128985

21. Bai Z, Williams RJ, Kitzler O, Sarang S, Spence DJ, Wang Y, et al. Diamond Brillouin laser in the visible. *APL Photon* (2020) 5(3):031301. doi:10.1063/1.5134907

22. Zheltikov A. High-peak-power nonlinear-optical processes in photonic crystal fibers. In: *Proceedings of the conference on lasers and electro-optics/quantum electronics and laser science conference and photonic applications systems technologies*. California: Long BeachOptica Publishing Group (2006). F 2006/05/21[C].

23. Boullet J, Zaouter Y, Desmarchelier R, Cazaux M, Salin F, Saby J, et al. High power ytterbium-doped rod-type three-level photonic crystal fiber laser. *Opt Express* (2008) 16(22):17891–902. doi:10.1364/oe.16.017891

24. Chen H, Bai Z, Wang J, Zhang B, Bai Z. Hundred-watt green picosecond laser based on LBO frequency-doubled photonic crystal fiber amplifier. *Infrared Laser Eng* (2021) 50(11):20200522. doi:10.3788/irla20200522

25. Reena D, Saini TS, Kumar A, Kalra Y, Sinha RK. Rectangular-core large-mode-area photonic crystal fiber for high power applications: Design and analysis. *Appl Opt* (2016) 55(15):4095–100. doi:10.1364/ao.55.004095

26. Limpert J, Schmidt O, Rothhardt J, Roser F, Schreiber T, Tunnermann A, et al. Extended single-mode photonic crystal fiber lasers. *Opt Express* (2006) 14(7):2715–20. doi:10.1364/oe.14.002715

27. Shi H, Song Y, Liang F, Xu L, Hu M, Wang C. Effect of timing jitter on time-of-flight distance measurements using dual femtosecond lasers. *Opt Express* (2015) 23(11):14057–69. doi:10.1364/oe.23.014057

28. Serafino G, Ghelfi P, Pérez-millán P, Villanueva GE, Palaci J, Cruz JL, et al. Phase and amplitude stability of EHF-band radar carriers generated from an active mode-locked laser. *J Lightwave Technol* (2011) 29(23):3551–9. doi:10.1109/jlt.2011.2170811

29. Hu S, Yu H, Duan Z, Zhu Y, Cao C, Zhou M, et al. Multi-parameter influenced acquisition model with an in-orbit jitter for inter-satellite laser communication of the LCES system. *Opt Express* (2022) 30(19):34362–77. doi:10.1364/oe.465592